Possible Superconductivity with a Bogoliubov Fermi Surface in a Lightly Doped Kagome U(1) Spin Liquid

Yi-Fan Jiang,[1,2] Hong Yao,[3,4,5,*] and Fan Yang[6,†]
[1]School of Physical Science and Technology, ShanghaiTech University, Shanghai 201210, China
[2]Stanford Institute for Materials and Energy Sciences, SLAC National Accelerator Laboratory and Stanford University, Menlo Park, California 94025, USA
[3]Institute of Advanced Study, Tsinghua University, Beijing 100084, China
[4]State Key Laboratory of Low Dimensional Quantum Physics, Tsinghua University, Beijing 100084, China
[5]Department of Physics, Stanford University, Stanford, California 94305, USA
[6]School of Physics, Beijing Institute of Technology, Beijing 100081, China

(Received 3 May 2020; revised 22 May 2021; accepted 30 September 2021; published 26 October 2021)

Whether the doped t-J model on the Kagome lattice supports exotic superconductivity has not been decisively answered. In this Letter, we propose a new class of variational states for this model and perform a large-scale variational Monte Carlo simulation on it. The proposed variational states are parameterized by the SU(2)-gauge rotation angles, as the SU(2)-gauge structure hidden in the Gutzwiller-projected mean-field Ansatz for the undoped model is broken upon doping. These variational doped states smoothly connect to the previously studied U(1) π-flux or 0-flux states, and energy minimization among them yields a chiral noncentrosymmetric nematic superconducting state with 2×2-enlarged unit cell. Moreover, this pair density wave state possesses a finite Fermi surface for the Bogoliubov quasiparticles. We further study experimentally relevant properties of this intriguing pairing state.

DOI: 10.1103/PhysRevLett.127.187003

Introduction.—Quantum spin liquids (QSL) have attracted increasing interest in condensed matter physics in the past decades [1–6]. They represent an exotic class of insulating states that cannot be adiabatically connected into a trivial band insulator. Moreover, a QSL state can support fractionalized excitations with fractional braiding statistics. One of the most intriguing aspects of QSL lies in that doping a QSL might naturally lead to high temperature superconductivity (SC) [7–16] or a topologically ordered Fermi liquid state (FL*) [17–19].

One promising model exhibiting a QSL ground state is the spin-1/2 Heisenberg model on the Kagome lattice, which is probably realized by the spin-liquid candidate material Herbertsmithite [3]. Numerous efforts have been devoted to studying the properties of this model for several decades. Except for a few early results pointing toward the valence bond solid state [20–22], dominating numerical results suggest a QSL ground state for this model [23–35]. Particularly, while a number of density-matrix renormalization group simulations on wide cylinders have exhibited evidence of a Z_2 QSL with exponentially decaying spin-spin correlation [23–28], recent infinite-size density-matrix renormalization group simulations on infinite cylinders [29], tensor-network simulations on infinite systems [30], and variational Monte Carlo (VMC) studies [31–33] suggest that the ground state is a gapless U(1) Dirac QSL with algebraic correlation. While further studies are still needed to reveal the precise nature of the ground state at half filling, it is also desirable to study what quantum state would be obtained when mobile charge carriers are introduced into the QSL state by doping. Specifically, can exotic superconductivity emerge upon doping the Kagome QSL state?

The nature of the lightly doped Kagome system described by the t-J model is not decisively known so far. Nonetheless, a recent density-matrix renormalization group study on the model with moderate doping on the 4-leg cylinder provided convincing evidence of an insulating holon Wigner crystal [36]. On the wider system, a previous VMC investigation of this model on up to $8^2 \times 9$ lattice in a certain doping range suggests that the π-flux Dirac U(1) spin liquid [31] is unstable against a 0-flux state with a valence bond crystal (VBC) ordering [37,38]. As the π-flux state has lower energy than the 0-flux state at half filling, it is obvious that the 0-flux state obtained by VMC at a certain doping range cannot be continuously connected to the undoped π-flux QSL state [31]. It is natural to ask what the ground state for the lightly doped t-J model on the Kagome lattice is, assuming that the ground state of the undoped system is a U(1) Dirac QSL.

In this Letter, we study the t-J model on the Kagome lattice in the very low doping regime, which is expected to smoothly connect with U(1) spin liquid at half filling [31], by performing VMC simulations. Our study is inspired by a crucial SU(2)-gauge structure [39–41] hidden in the projective construction at half filling: two different

mean-field (MF) Ansätze related by an arbitrary local SU(2)-gauge rotation actually correspond to the same physical spin state after the Gutzwiller projection. Such gauge redundancy leads to a many-to-one labeling between the mean-field Ansätze and the projected wave function at half filling [42]. At finite doping, the breaking of this gauge structure differentiates the many states related by the gauge rotation, which form our variational groups. We choose the doped 0-flux or π-flux states as our unrotated starting points. Energy minimizations within both groups of variational states yield chiral noncentrosymmetric nematic superconducting states with 2×2-enlarged unit cell in the very low doping regime, with the gauge-rotated π-flux state smoothly connecting to the undoped π-flux QSL [31]. Remarkably, as the SU(2)-gauge rotation maintains the quasiparticle spectrum, the obtained superconducting states possess finite Fermi surface (FS) for the Bogoliubov quasiparticles. The physical properties of these pairing states are intriguing: although they are superconducting states, they resemble those of the normal FL in many aspects.

Variational states.—We study the standard t-J model on the Kagome lattice illustrated in Fig. 1(a):

$$H = -t\sum_{\langle ij\rangle\sigma} P_G(c^\dagger_{i\sigma}c_{j\sigma} + \text{H.c.})P_G + J\sum_{\langle ij\rangle}\left(\mathbf{S}_i\cdot\mathbf{S}_j - \frac{1}{4}n_i n_j\right), \tag{1}$$

where $c_{i\sigma}$ annihilates an electron on site i with spin σ, $\mathbf{S}_i = \frac{1}{2}c^\dagger_{i\alpha}\boldsymbol{\sigma}_{\alpha\beta}c_{i\beta}$ denotes the spin operator, and $n_i = \sum_\sigma c^\dagger_{i\sigma}c_{i\sigma}$ is the density operator. $P_G = \prod_i(1 - n_{i\uparrow}n_{i\downarrow})$ is the Gutzwiller-projection operator enforcing a no-double-occupancy constraint. $\langle ij\rangle$ represents nearest-neighbor (NN) bonding. Here, we set $J = 1$ as the energy scale. The parameter t and the doping concentration δ are set as tuning parameters spanning the phase diagram.

To smoothly connect with the previously studied π-flux state at half filling [31] and to compare energy with the 0-flux state at finite doping [37,38], we investigate the Gutzwiller-projected MF states generated by the following MF Hamiltonian:

$$H^0_{\text{MF}} = \sum_{\langle ij\rangle\sigma}\chi_{ij}c^\dagger_{i\sigma}c_{j\sigma} + \text{H.c.}, \tag{2}$$

where $\chi_{ij} = \pm 1$. These states can be characterized by the fluxes $e^{i\phi} = \prod_{\text{plaquette}}\text{sgn}(\chi_{ij})$ through triangle and hexagon plaquettes of the Kagome lattice. In this work, we primarily focus on two types of fluxes: (1) the 0-flux states having zero flux through all the triangles and hexagons shown in Fig. 1(b); (2) the π-flux state having π flux through the hexagons and zero flux through the triangles as shown in Fig. 1(c). At half filling, both flux states after the projection are QSL. While the former has a large spinon FS, the latter is a U(1) Dirac QSL. Previous VMC studies [31] showed that the π-flux state has the lowest energy among all studied states.

The key point lying behind the present work is the following SU(2)-gauge structure hidden in the projective construction at half filling [40,41]. Let us perform the following local SU(2)-gauge transformation W_i on the two component spinor $\psi_i = (c_{i\uparrow}, c^\dagger_{i\downarrow})^T$:

$$\begin{bmatrix} c_{i\uparrow} \\ c^\dagger_{i\downarrow}\end{bmatrix} \to W_i \begin{bmatrix} c_{i\uparrow} \\ c^\dagger_{i\downarrow}\end{bmatrix}. \tag{3}$$

At half filling, any two MF Ansätze connected by this local SU(2)-gauge rotation label the same physical spin state after projected into the single-occupance subspace, as the spin operator $\mathbf{S}_i$ keeps invariant under this gauge transformation [40,41]. However, this many-to-one labeling is absent once the system is doped away from half filling. Consequently, the many states related by the gauge rotation before projection can represent physical states with distinct physical properties at finite doping. One may naturally raise the following question: what is the lowest-energy state among all those gauge-rotated π- or 0-flux states for the system with very low doping? To answer this question, we choose the local SU(2)-gauge rotation angles as variational parameters, from which we construct an MF Hamiltonian to generate the variational physical states by projection, for energy minimization in both flux sectors.

Our trial wave functions are generated by the following local SU(2)-gauge-rotated Bogoliubov–de Genes MF Hamiltonian:

$$H_{\text{MF}} = \sum_{ij}[\,c^\dagger_{i\uparrow} \quad c_{i\downarrow}\,]W_i\begin{bmatrix}\chi_{ij} & 0 \\ 0 & -\chi_{ji}\end{bmatrix}W^\dagger_j\begin{bmatrix} c_{j\uparrow} \\ c^\dagger_{j\downarrow}\end{bmatrix}. \tag{4}$$

Here, the unrotated MF parameter χ_{ij} on the NN bond $\langle ij\rangle$ for the π- and 0-flux states have been introduced above. We set the on-site term χ_{ii} to a uniform value $\chi_{ii} = \chi_0$ as the chemical potential term. The local SU(2) rotation matrix W_i

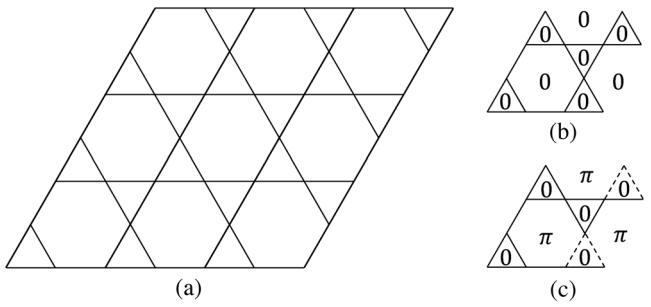

FIG. 1. (a) A schematic representation of the Kagome lattice. (b) The 0-flux state with $\chi_{ij} = 1$ on each bond. (c) The π-flux state with zero flux through triangles and π-flux through hexagonals. Dashed lines indicate the $\chi = -1$ bonds.

can be parameterized by the following three rotation angles, α_i, β_i, and γ_i, as

$$W_i = \begin{bmatrix} e^{i\beta_i}\cos\alpha_i & e^{i\gamma_i}\sin\alpha_i \\ -e^{-i\gamma_i}\sin\alpha_i & e^{-i\beta_i}\cos\alpha_i \end{bmatrix}. \quad (5)$$

Our trial wave function $P_G|\Psi_{\mathrm{MF}}\{\chi_0,\alpha,\beta,\gamma\}\rangle$ now depends on the set of variational parameters $\{\alpha_i,\beta_i,\gamma_i\}_{i=1,\ldots,N}$ and χ_0. Here, $|\Psi_{\mathrm{MF}}\{\chi_0,\alpha,\beta,\gamma\}\rangle$ is the MF ground state of Eq. (4).

VMC results.—We adopt a standard Monte Carlo approach to simulate the variational states $P_G|\Psi_{\mathrm{MF}}\{\chi_0,\alpha,\beta,\gamma\}\rangle$ on the Kagome lattice with size $3\times L\times L$ and periodic boundary condition, where the two adopted lattice sizes $L=8$ and $L=12$ lead to consistent results. The numerical complexity arising from optimizing a large number of variational parameters is overcome by the stochastic reconfiguration method [43]. We further reduce the number of SU(2) rotation angles by restricting the parameters in the supercell with size $3\times 2\times 2$. We have checked that increasing the size of the supercell does not lead to a lower optimized energy (see the Supplemental Material (SM) [44] for detail).

Our main results are summarized in the phase diagram shown in Fig. 2(a), where we consider several t ranging from $1/3$ to 3 and several doping levels below 7% on the Kagome lattice with $L=8$. Starting from the undoped π-flux state, the lowest-energy state stays in the π-flux sector until beat by the optimized states in 0-flux sector at a finite doping concentration δ_c depending on t. For small $t\sim 1/3$, the gauge-rotated π-flux state is stable until the doping concentration reaches $\delta_c\sim 5\%$. While for large t, a smaller doping is enough to drive the system away from the π-flux sector, consistent with previous VMC studies at $J=0.4t$ [37,38]. To explore the possible finite size effect, we also studied the models on $L=12$ lattice with 4 to 12

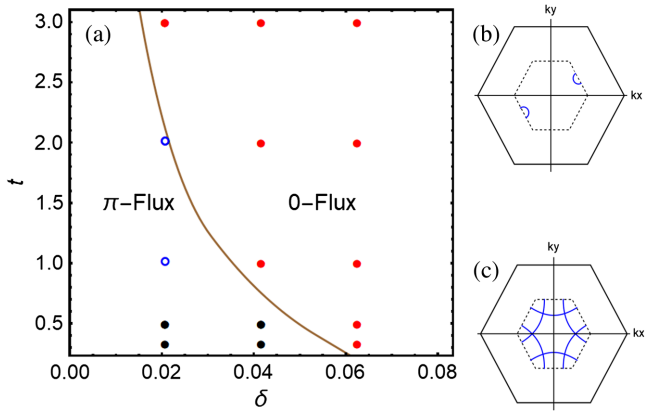

FIG. 2. (a) Phase diagram of the slightly doped t-J model on an $8\times 8\times 3$ lattice. The black circles in the π-flux sector represent metallic phase without pairing. (b) Nearly doubly degenerate small FSs of the slightly doped π-flux state located around the two folded Dirac points of undoped state. (c) Folded FSs of the doped 0-flux state.

doped holes and found that the gauge-rotated π-flux state is still the lowest-energy state for most of the cases at small doping region.

The physical properties of the gauge-rotated π-flux phase are mainly determined by the optimized SU(2) rotation angles, which are provided in the SM [44]. Except for the two parameter points in the small J and δ region of the π-flux sector (black circles in Fig. 2), we find that the optimized angle α_i for both flux sectors are neither 0 nor π. Consequently, the nonzero off-diagonal terms in the gauge-rotation matrices W_i defined in Eq. (5) bring about a singlet pairing term $H_\Delta=-\sum_{ij}c^\dagger_{i\uparrow}c^\dagger_{j\downarrow}[\chi_{ij}e^{i(\beta_i+\gamma_j)}\cos\alpha_i\sin\alpha_j+(i\rightleftarrows j)]+\mathrm{H.c.}$ in H_{MF}. Note that the gauge rotation [Eq. (3)] as a unitary transformation does not change the quasiparticle spectra [40,41] but only leads to enlargement of the unit cell. As a result, the superconducting states generated here will have quasiparticle FSs simply folded from those of the doped 0- or π-flux states before the gauge rotation, as shown in Figs. 2(b) and 2(c). Therefore, we have obtained here singlet pairing states with finite Bogoliubov FS. Such SC states breaking translational symmetry with finite FS were pair-density-wave states [45–59].

The optimized gauge-rotation angles in the π-flux sector are complicated because all the $\{\alpha_i,\beta_i,\gamma_i\}$ within the supercell are nonzero and nonuniform, breaking the time reversal symmetry (TRS), the lattice rotation, the inversion, and the translational symmetries. The pairing and hopping terms generated by the gauge rotations are generally complex and are of the same order of magnitude, which suggests a typical interband pairing state. More details of the optimized gauge-rotation angles and the resulting gauge-rotated MF Hamiltonian are provided in the SM [44]. In spite of the complicated pairing and hopping terms, the resulting MF Hamiltonian exhibits the finite Bogoliubov FS shown in Fig. 2(b), which comprises two nearly doubly degenerate small pockets folded from those of the unrotated π-flux state.

At infinitesimal doping, the gauge-rotated π-flux state is reasonably the lowest-energy VMC state due to the finite energy difference between this state and other states presented in the previous VMC study of the undoped case. When the doping concentration becomes larger, besides the gauge-rotated π- or 0- flux states, other competitive states such as the holon Wigner crystal [36], the doped Z_2 QSL [34], various types of VBC states [37,38], and the uniform-pairing states [7,60,61] should also be considered in the VMC calculations. In Table I, we list the optimized energies for part of the lowest-energy states we obtained on the $L=12$ lattice, which suggests that in the small doping region the gauge-rotated π-flux state has lower energy than the other VMC candidates. We can see the doped Z_2 QSL [34] provides similar energy as the gauge-rotated π-flux state because after optimization such state actually flows back to the U(1) Dirac spin liquid

TABLE I. Optimized energy of part of the candidates on the model with $t = 0.5 \sim 2$ and $\delta = 0.92\% \sim 2.78\%$ on a $3 \times 12 \times 12$ lattice. A complete table with more candidate Ansätze can be found in the SM [44].

		$\delta = 0.92\%$	$\delta = 1.85\%$	$\delta = 2.78\%$
t = 2	0-flux	−0.96 037(2)	−1.008 73(3)	−0.56 69(3)
	π-flux	−0.971 05(5)	−1.011 97(2)	−1.052 38(3)
	Z_2 QSL	−0.971 06(2)	−1.011 96(4)	−1.052 31(4)
	VBC-D	−0.960 66(3)	−1.009 21(2)	−1.057 10(3)
	CDW	−0.9112(3)	/	/
t = 1	0-flux	0.928 94(3)	−0.946 80(1)	−0.964 08(2)
	π-flux	−0.943 47(2)	−0.956 91(2)	−0.970 10(4)
	Z_2 QSL	−0.943 48(3)	−0.956 86(4)	−0.970 10(3)
	VBC-D	0.929 33(2)	0.946 98(2)	−0.964 42(2)
	CDW	−0.9104(4)	/	/
t = 0.5	0-flux	−0.913 36(4)	−0.915 65(3)	−0.917 72(3)
	π-flux	−0.929 67(3)	−0.929 39(2)	−0.928 28(2)
	Z_2 QSL	−0.929 65(2)	−0.929 36(3)	−0.928 27(3)
	VBC-D	−0.913 67(2)	−0.915 88(3)	−0.918 08(2)
	CDW	−0.9154(2)	/	/

(π-flux state) for all the cases we studied. In the 0-flux sector, we find that the D-type VBC state has slightly lower energy than the gauge-rotated 0-flux state. Another important candidate, the holon Wigner crystal, is mimicked by the charge density wave (CDW) Ansatz in the VMC calculation. Restricted by the finite lattice size, we only consider the four-hole doped $L = 12$ system with $3 \times 6 \times 6$ supercell. Though we observe the similar density distribution as the Wigner crystal, the VMC energy of this CDW state is higher than the gauge-rotated π-flux state. We also consider the uniform-pairing states with both the extended s-wave and d-wave pairing parameters live on the nearest and second nearest neighbor bonds, which also provide higher energies in the small doping region. We considered a more complete comparison of all the competing states on the $L = 12$ lattice, and the detailed VMC realization of them is presented in the SM [44].

Singlet pairing with finite FS.—The singlet pairing with Bogoliubov FS obtained here is distinct from conventional superconductors. To reveal the physical properties of this intriguing pairing state relevant to experiments, we shall perform MF studies below toward the zero- and finite-temperature behaviors of the system represented by the optimized H_{MF}. Consequently, this pairing state is found to be very exotic.

On one hand, the breaking of U(1)-gauge symmetry leads to finite superfluid density as expected (see the SM [44] for details), which will result in detectable Meissner effect. On the other hand, the presence of the full FS causes finite density of state that, in combination with the singlet-pairing signature, makes this pairing state look like a normal FL in the aspects of low lying quasiparticle and

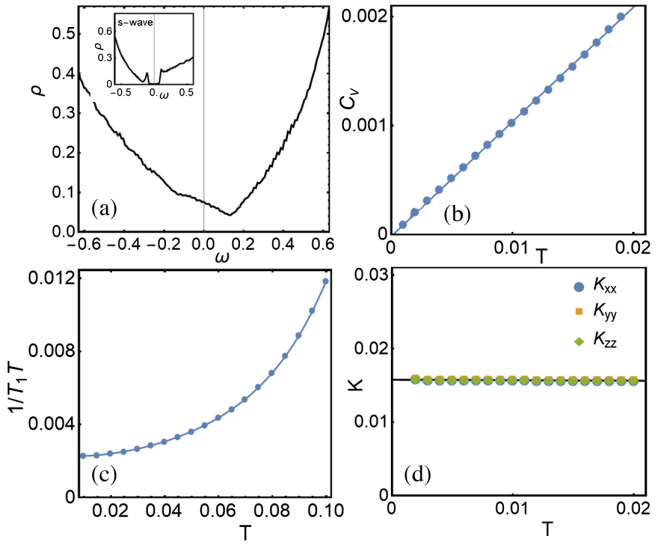

FIG. 3. Experiment-relevant quantities for the optimized gauge-rotated π-flux state. (a) $dI/dV \sim V$ curve for the STM. The inset is the dI/dV curve for the model with uniform on-site s wave. (b) The specific heat $C_v \sim T$. (c) The NMR relaxation rate $1/T_1T$. (d) The NMR Knight-shift K as function of T; the three colors stand for K_{xx}, K_{yy}, and K_{zz}, respectively. The optimal gauge-rotation angles are obtained from parameter setting $t = 0.5$ and $\delta = 2.08\%$.

spin excitations, as shown in Fig. 3 for the gauge-rotated π-flux state. In the zero-temperature dI/dV curve for the STM spectrum shown in Fig. 3(a), a finite zero-bias conductance appears caused by the finite density of state in comparison with the U-shaped curve for the s-wave SC shown in the inset. Figure 3(b) shows that the specific heat $C_v \propto T$ at $T \to 0$, resembling the normal FL. Figure 3(c) illustrates that the relaxation rate $1/T_1T$ of the nuclear magnetic resonance (NMR) saturates to a finite value at $T \to 0$, obeying a Korringa-law-like behavior for the FL, different from the $1/T_1T \to 0$ behavior for conventional fully gapped ($\propto e^{-\Delta/T}$) or nodal ($\propto T^3$) SC. Figure 3(d) exhibits that the NMR Knight-shift K saturates to a finite value for $T \to 0$, independent of the orientation of the exerted magnetic field, similarly to the Pauli-susceptibility behavior for standard FL. This behavior is distinct from the $K \to 0$ behavior of conventional singlet SC with full or nodal gap or the obvious magnetic field orientation dependence of K for the triplet SC. Although both the gauge-rotated π- or 0- flux states exhibit Bogoliubov FS, the different doping dependences of the area enclosed by their FSs can be distinguished by the angle-resolved photoemission spectroscopy, which can also lead to different behaviors such as the doping dependence of C_v/T. Details of these MF studies are provided in the SM [44].

Discussion and conclusion.—Note that, starting with a U(1) QSL at half filling, we have only considered the gauge-rotation angles as variational parameters and neglect the amplitude fluctuation of χ_{ij} before the gauge rotation.

Such a treatment is reasonable only at zero-doping limit. For higher dopings, lower variational energy is generally expected if we include the variation of the amplitude of χ_{ij}. The band structure of such improved state can be strongly modified, i.e., a Hastings-type VBC order can gap out the Dirac points [62]. We have briefly investigated the fate of the Hastings-type VBC in the unrotated π-flux state and found that it becomes visible when the doping concentration is larger than $\delta_c \sim 4\%$. Therefore, close to the zero-doping limit, the Bogoliubov FS is more likely to survive.

Previous studies [63–67] have shown the survival of the FS under the Gutzwiller projection, although some other MF properties might be modified [68], such as the quasiparticle weight. A similar phenomenon, namely the survival of the FS under Gutzwiller projection, is also directly observed for our projected gauge-rotated states by numerically detecting the FS jump in the occupation-number distribution of Bogoliubov quasiparticles in the momentum space (see the SM for details [44]). Another concern about the stability of the Bogoliubov FS obtained here under possible remnant interactions among the Bogoliubov quasiparticles is neglected in the VMC treatment. Indeed, the FSs shown in Figs. 2(b) and (c) atisfy the relation $\varepsilon_{\mathbf{k}} = \varepsilon_{-\mathbf{k}}$ as the unitary SU(2)-gauge rotation adopted here maintains the quasiparticle energy, which will suffer from the Cooper instability under remnant interactions. However, note that the two superconducting states obtained here break both the TRS and the inversion symmetry [44]. Without the protection of these two symmetries [69], the relation $\varepsilon_{\mathbf{k}} = \varepsilon_{-\mathbf{k}}$ cannot survive such perturbations as the further variations of $\{\chi_{ij}, \Delta_{ij}\}$ after the gauge rotation, which can always exist for finite doping. Consequently, the Bogoliubov FSs obtained here should be stable against weak remnant interactions among the quasiparticles.

Evidence of SC with Bogoliubov FS can also appear in other contexts such as the Fulde-Ferrell-Larkin-Ovchinnikov state induced in the magnetic field [70,71], the cubic system with $j = 3/2$ total angular momentum degree of freedom [72], and some iron-based superconductors with spin-orbit coupling and interband pairing [73]. The recently synthesized YPtBi multiband superconductor with strong spin-orbit coupling [74,75] might also exhibit Bogoliubov FS if it breaks the TRS [76]. While these systems host similar normal FL-like quasiparticle excitations as here, their spin excitations have different properties from those of the singlet pairing state obtained here. In summary, we propose a new way to obtain the Bogoliubov FS: doping a U(1) QSL. The key point lies in the fact that the local SU(2)-gauge rotation, which brings about SC to the doped QSL, will not alert the quasiparticle energy, which is different from doping a QSL with spinon FS [77]. Such mechanism not only applies to the doped Kagome U(1) QSL but also applies to other doped U(1) QSL, which could be a promising way to obtain the new type of unconventional gapless SC in strongly correlated electronic systems.

We are grateful to the helpful discussions with T. Li, Y.-M. Lu, Y. Zhou, W.-Q. Chen, Z.-C. Gu, and Z.-Y. Weng. This work is supported in part by the start-up grant of ShanghaiTech University (Y. F. J.), the NSFC Grant No. 11825404 (H. Y.), the NSFC Grant No. 12074031 (F. Y.), the MOSTC Grant 2018YFA0305604 (H. Y.), the Strategic Priority Research Program of Chinese Academy of Sciences under Grant No. XDB28000000 (H. Y.), the Beijing Municipal Science and Technology Commission under Grant No. Z181100004218001 (H. Y.), and the Beijing Natural Science Foundation under Grant No. Z180010 (H. Y.). Y. F. J. would also like to acknowledge support in part by the Department of Energy, Office of Science, Basic Energy Sciences, Materials Sciences and Engineering Division, under Contract No. DE-AC02-76SF00515. H. Y. would also like to acknowledge support in part by the Gordon and Betty Moore Foundations EPiQS Initiative through Grant No. GBMF4302. Parts of the computing for this work was performed on the Sherlock cluster.

*Corresponding author.
yaohong@tsinghua.edu.cn
†Corresponding author.
yangfan_blg@bit.edu.cn

[1] P. W. Anderson, Mater. Res. Bull. **8**, 153 (1973).
[2] Y. Zhou, K. Kanoda, and T.-K. Ng, Rev. Mod. Phys. **89**, 025003 (2017).
[3] M. R. Norman, Rev. Mod. Phys. **88**, 041002 (2016).
[4] P. A. Lee, N. Nagaosa, and X.-G. Wen, Rev. Mod. Phys. **78**, 17 (2006).
[5] C. Broholm, R. J. Cava, S. A. Kivelson, D. G. Nocera, M. R. Norman, and T. Senthil, Science **367**, eaay0668 (2020).
[6] L. Balents, Nature (London) **464**, 199 (2010).
[7] P. W. Anderson, Science **235**, 1196 (1987).
[8] S. A. Kivelson, D. S. Rokhsar, and J. P. Sethna, Phys. Rev. B **35**, 8865 (1987).
[9] D. S. Rokhsar and S. A. Kivelson, Phys. Rev. Lett. **61**, 2376 (1988).
[10] R. B. Laughlin, Science **242**, 525 (1988).
[11] X. G. Wen, F. Wilczek, and A. Zee, Phys. Rev. B **39**, 11413 (1989).
[12] X.-G. Wen and P. A. Lee, Phys. Rev. Lett. **76**, 503 (1996).
[13] S. S. Lee, P. A. Lee, and T. Senthil, Phys. Rev. Lett. **98**, 067006 (2007).
[14] E. Fradkin, S. A. Kivelson, and J. M. Tranquada, Rev. Mod. Phys. **87**, 457 (2015).
[15] H.-C. Jiang, npj Quantum Mater. **6**, 71 (2021).
[16] Y.-F. Jiang and H.-C. Jiang, Phys. Rev. Lett. **125**, 157002 (2020).
[17] T. Senthil, S. Sachdev, and M. Vojta, Phys. Rev. Lett. **90**, 216403 (2003).
[18] M. Punk, A. Allais, and S. Sachdev, Proc. Natl. Acad. Sci. U.S.A. **112**, 9552 (2015).
[19] A. A. Patel, D. Chowdhury, A. Allais, and S. Sachdev, Phys. Rev. B **93**, 165139 (2016).

[20] R. R. P. Singh and D. A. Huse, Phys. Rev. B **76**, 180407(R) (2007).
[21] R. R. P. Singh and D. A. Huse, Phys. Rev. B **77**, 144415 (2008).
[22] G. Evenbly and G. Vidal, Phys. Rev. Lett. **104**, 187203 (2010).
[23] H. C. Jiang, Z. Y. Weng, and D. N. Sheng, Phys. Rev. Lett. **101**, 117203 (2008).
[24] S. Yan, D. Huse, and S. White, Science **332**, 1173 (2011).
[25] H. C. Jiang, Z. Wang, and L. Balents, Nat. Phys. **8**, 902 (2012).
[26] S. Depenbrock, I. P. McCulloch, and U. Schollwöck, Phys. Rev. Lett. **109**, 067201 (2012).
[27] S.-S. Gong, W. Zhu, L. Balents, and D. N. Sheng, Phys. Rev. B **91**, 075112 (2015).
[28] J.-W. Mei, J.-Y. Chen, H. He, and X.-G. Wen, Phys. Rev. B **95**, 235107 (2017).
[29] Y.-C. He, M. P. Zaletel, M. Oshikawa, and F. Pollmann, Phys. Rev. X **7**, 031020 (2017).
[30] H. J. Liao, Z. Y. Xie, J. Chen, Z. Y. Liu, H. D. Xie, R. Z. Huang, B. Normand, and T. Xiang, Phys. Rev. Lett. **118**, 137202 (2017).
[31] Y. Ran, M. Hermele, P. A. Lee, and X. G. Wen, Phys. Rev. Lett. **98**, 117205 (2007).
[32] Y. Iqbal, F. Becca, S. Sorella, and D. Poilblanc, Phys. Rev. B **87**, 060405(R) (2013).
[33] Y. Iqbal, D. Poilblanc, and F. Becca, Phys. Rev. B **89**, 020407(R) (2014).
[34] T. Li, arXiv:1807.09463.
[35] H. J. Changlani, D. Kochkov, K. Kumar, B. K. Clark, and E. Fradkin, Phys. Rev. Lett. **120**, 117202 (2018).
[36] H.-C. Jiang, T. Devereaux, and S. A. Kivelson, Phys. Rev. Lett. **119**, 067002 (2017).
[37] S. Guertler and H. Monien, Phys. Rev. B **84**, 174409 (2011).
[38] S. Guertler and H. Monien, Phys. Rev. Lett. **111**, 097204 (2013).
[39] G. Baskaran and P. W. Anderson, Phys. Rev. B **37**, 580(R) (1988).
[40] I. Affleck, Z. Zou, T. Hsu, and P. W. Anderson, Phys. Rev. B **38**, 745 (1988).
[41] E. Dagotto, E. Fradkin, and A. Moreo, Phys. Rev. B **38**, 2926 (1988).
[42] X.-G. Wen, Phys. Rev. B **65**, 165113 (2002).
[43] S. Sorella, Phys. Rev. B **71**, 241103(R) (2005).
[44] See Supplemental Material at http://link.aps.org/supplemental/10.1103/PhysRevLett.127.187003 for the formula of the SU(2)-gauge rotated mean-field Hamiltonian; the realization and optimized energy of the holon Wigner crystal, the doped Z_2 QSL, various types of VBC states, and the uniform-pairing states; the optimized results of the SU(2)-gauge-rotation angles for the doped π- or 0-flux states; the formula for the calculations of the STM, the specific heat, the Knight-shift, the NMR relaxation rate, and the zero- and finite-temperature superfluid density.
[45] E. Berg, E. Fradkin, E.-A. Kim, S. A. Kivelson, V. Oganesyan, J. M. Tranquada, and S. C. Zhang, Phys. Rev. Lett. **99**, 127003 (2007).
[46] D. F. Agterberg and H. Tsunetsugu, Nat. Phys. **4**, 639 (2008).
[47] E. Berg, E. Fradkin, and S. A. Kivelson, Nat. Phys. **5**, 830 (2009).
[48] E. Berg, E. Fradkin, S. A. Kivelson, and J. M. Tranquada, New J. Phys. **11**, 115004 (2009).
[49] E. Berg, E. Fradkin, and S. A. Kivelson, Phys. Rev. Lett. **105**, 146403 (2010).
[50] A. Jaefari and E. Fradkin, Phys. Rev. B **85**, 035104 (2012).
[51] P. A. Lee, Phys. Rev. X **4**, 031017 (2014).
[52] S.-K. Jian, Y.-F. Jiang, and H. Yao, Phys. Rev. Lett. **114**, 237001 (2015).
[53] M. H. Hamidian, S. D. Edkins, S. H. Joo, A. Kostin, H. Eisaki, S. Uchida, M. J. Lawler, E.-A. Kim, A. P. Mackenzie, K. Fujita, J. Lee, and J. C. S. Davis, Nature (London) **532**, 343 (2016).
[54] W. Ruan, X. Li, C. Hu, Z. Hao, H. Li, P. Cai, X. Zhou, D.-H. Lee, and Y. Wang, Nat. Phys. **14**, 1178 (2018).
[55] S. D. Edkins, A. Kostin, K. Fujita, A. P. Mackenzie, H. Eisaki, S. Uchida, S. Sachdev, M. J. Lawler, E.-A. Kim, J. C. S. Davis, and M. H. Hamidian, Science **364**, 976 (2019).
[56] S.-K. Jian, M. M. Scherer, and H. Yao, Phys. Rev. Research **2**, 013034 (2020).
[57] Z. Han, S. A. Kivelson, and H. Yao, Phys. Rev. Lett. **125**, 167001 (2020).
[58] K. S. Huang, Z. Han, S. A. Kivelson, and H. Yao, arXiv:2103.04984.
[59] D. F. Agterberg, J. S. Davis, S. D. Edkins, E. Fradkin, D. J. Van Harlingen, S. A. Kivelson, P. A. Lee, L. Radzihovsky, J. M. Tranquada, and Y. Wang, Annu. Rev. Condens. Matter Phys. **11**, 231 (2020).
[60] C. Gros, Phys. Rev. B **38**, 931 (1988).
[61] P. W. Anderson, M. Randeria, T. Rice, N. Trivedi, and F. Zhang, J. Phys. Condens. Matter **16**, R755 (2004).
[62] M. B. Hastings, Phys. Rev. B **63**, 014413 (2000).
[63] A. Paramekanti, M. Randeria, and N. Trivedi, Phys. Rev. Lett. **87**, 217002 (2001).
[64] A. Paramekanti, M. Randeria, and N. Trivedi, Phys. Rev. B **70**, 054504 (2004).
[65] S. Yunoki, Phys. Rev. B **72**, 092505 (2005).
[66] C. P. Nave, D. A. Ivanov, and P. A. Lee, Phys. Rev. B **73**, 104502 (2006).
[67] H.-Y. Yang, F. Yang, Y.-J. Jiang, and T. Li, J. Phys. Condens. Matter **19**, 016217 (2007).
[68] F. Ferrari and F. Becca, Phys. Rev. X **9**, 031026 (2019).
[69] M. Barkeshli, H. Yao, and S. A. Kivelson, Phys. Rev. B **87**, 140402(R) (2013).
[70] P. Fulde and R. A. Ferrell, Phys. Rev. **135**, A550 (1964).
[71] A. I. Larkin and Y. N. Ovchinnikov, Zh. Eksp. Teor. Fiz. **47**, 1136 (1964).
[72] D. F. Agterberg, P. M. R. Brydon, and C. Timm, Phys. Rev. Lett. **118**, 127001 (2017).
[73] C. Setty, S. Bhattacharyya, Y. Cao, A. Kreisel, and P. J. Hirschfeld, Nat. Commun. **11**, 523 (2020).
[74] P. M. R. Brydon, L. M. Wang, M. Weinert, and D. F. Agterberg, Phys. Rev. Lett. **116**, 177001 (2016).
[75] H. Kim, K. Wang, Y. Nakajima, R Hu, S. Ziemak, P. Syers, L Wang, H. Hodovanets, J. D. Denlinger, P. M. R. Brydon, D. F. Agterberg, M. A. Tanatar, R. Prozorov, and J. Paglione, Sci. Adv. **4**, eaao4513 (2018).
[76] C. Timm, A. P. Schnyder, D. F. Agterberg, and P. M. R. Brydon, Phys. Rev. B **96**, 094526 (2017).
[77] X. Y. Xu, K. T. Law, and P. A. Lee, Phys. Rev. Lett. **122**, 167001 (2019).